Design of Flat Oval LDSS Stub Columns of Slender Cross-Sections

Khwairakpam Sachidananda and Konjengbam Darunkumar Singh

Department of Civil Engineering, Indian Institute of Technology Guwahati, India

Abstract

In this paper, parametric study on the structural behaviour (e.g. deformation modes, load capacity) of fixed ended lean duplex stainless steel (LDSS) flat oval hollow section stub columns, is presented, considering variation of l_f (flat element length), r (radius of curved element), t (thickness), keeping w (flat element spacing) and h (height of column) constant, using the finite element (FE) software Abaqus. Based on the study, an expression has been proposed for calculating the effective thickness of curved elements of slender ($w/t \geq 40$) sections, for reliable load capacity predictions when used with ASDM, AS/NZS 4673, ASCE 8-02 and EN 1993-1-4 equations.

Keywords

LDSS, Abaqus, Flat-oval, Finite element, stub column, AS/NZS 4673, ASCE 8-02, EN 1993-1-4, ASDM.

1 Introduction

In the tubular steel construction industry, cross-sectional shapes such as square, rectangular and circular are mainly used owing to their well researched nature with considerable design guidelines available in the literature and codes. However, recently, as architects and engineers attempted to explore innovative steel cross sectional shapes, especially for exposed architectural applications, new cross sections such as elliptical, oval, etc. were introduced in the market. The use of such oval / elliptical sections can be seen in popular places like Legends center, Canada, Electronics arts stairwell, Canada (Haque, 2011), Barajas airport, Spain; Heathrow airport, UK; Cork airport, Ireland; Zeeman building, University of Warwick, UK, Society bridge, Scotland (Chan *et al*., 2010) etc. Additionally, of late, a new type of cross section known as flat-oval section has been introduced in the market (e.g. Form 220 and 370 flat oval from Rukki, 2017). Flat-oval section is an interesting cross section, essentially due to the combination of flat and curve elements. Earlier study on flat-oval (consisting of flat and semi-circular sections) steel sections was notably initiated by Parks and Yu (1987, 1989), who reported on both analytical and experimental investigations on the interaction effect of curved and flat elements of stiffened bolted flat oval steel stub columns. Later, Zhu and Young (2011, 2012) reported both experimental and finite element work on cold formed flat oval hollow steel sections (a single section made of two flat web and two rounded semi-circular flange faces) columns under compression. Effects of cross sectional parameters for Lean duplex Stainless Steel (LDSS) columns were reported by the authors (Sachidananda and Singh, 2015; 2017), using finite element analysis. It may be noted that current structural steel design codes are not specific on the design of section consisting of flat and curve elements such as flat oval sections. The current finite element study presents an extension of the authors' earlier work (Sachidananda and Singh, 2015; 2017) for non-compact (or slender) sections with $w/t \geq 40$ (w = width between flat elements, t = thickness). The results of the study are then compared with predictions from EN 1993-1-4 (2015) and AS/NZS 4673 (2001)/ASCE 8-02 (2002), and ASDM (2002). Further, in this paper, possible modifications to EN 1993-1-4 (2015), AS/NZS 4673 (2001)/ASCE 8-02(2002) and ASDM (2002) are also presented for reliable load capacity predictions.

2 Finite Element (FE) Modelling

2.1 General

Typical cross-section of flat oval is shown in Fig. 1 where l_f, r, w, h represent flat length, curvature radius, width between flat plates, length of columns. In the current study, the structural behaviour of fixed ended LDSS flat oval hollow stub column were investigated using the general purpose finite element (FE) software, considering variation of key cross sectional parameters *viz.*, r (radius of curved element), l (flat element length), t (thickness), keeping w (width between flat elements) and h (column height) as constants (w = 300 mm, h = 900 mm). Both local imperfections and material non-linearity were considered in the FE models. The first part of the study, involves the validation of the FE modeling approach by comparing with experimental results of LDSS square hollow section columns under axial compression (Theofanous and Gardner, 2009). After validation, parametric study of the fixed ended LDSS flat oval hollow stub columns are presented. The basic FE modeling approaches adopted in the present study are summarized in the following sub-sections. The shell FE procedure followed in this paper are those typically adopted for the study of thin walled metallic structures (see e.g., Zhu and Young (2012) for cold-formed flat-oval sections, Chan and Gardner (2008) for hot-rolled elliptical sections, Gardner and Ministro (2004) for oval sections, Patton and Singh (2012) for LDSS L, T, and + sections, Sachidananda and Singh (2015) for LDSS flat-oval sections, Saliba and Gardner (2013) for LDSS I-sections etc.).

Paper presented by Konjengbam Darunkumar Singh - darun@iitg.ernet.in

2.2 Geometry and boundary conditions

In order to established fixed ended conditions, the bottom part is fixed while the top part is allowed to move in the axial direction. This boundary condition was achieved by providing reference points, RP1 and RP2, which constraints the column ends *via* kinematic coupling (Abaqus, 2009), as shown in Fig. 2. Similar approach was followed in Lui and Young (2003), Ellobody and Young (2005), Theofanous and Gardner (2009), Patton and Singh (2012), Gardner and Ashraf (2006), Gardner and Ministro (2004) etc. The geometric parameters of stub columns are in the range: r = 150-750 mm, l_f = 300-700 mm and t = 3-7.5 mm.

2.3 Finite element mesh

The FE models were meshed with four-noded doubly curved shell element having six degrees of freedom per node with reduced integration scheme ('S4R' elements in Abaqus terminology). It may be noted that S4R elements are generally reported in the literature to provide good results for modelling metallic thin walled members under different loading conditions (e.g. Theofanous and Gardner, 2009, Ellobody and Young, 2005, Chan and Gardner, 2008). Based on the mesh convergence study, using linear elastic eigen buckling analysis, a squarish element of size range 8-10 mm were adopted for the FE models. A typical FE mesh for LDSS flat oval hollow column is shown in Fig. 2.

2.4 Geometric imperfection

In order to mimic local surface imperfections, associated with real life steel tubular members (resulting from manufacturing, fabrication, transportation, storage etc.), the perfect FE models are seeded with local imperfections shapes. The seeded local imperfections are derived from linear elastic eigen buckling analysis, by scaling with local imperfection amplitude of t/100, where t is the thickness (see e.g. Theofanous *et al*. (2009), Chan and Gardner (2008), Patton and Singh (2012)).

2.5 Material modeling

For modelling the stress-strain material property of the LDSS, a two stage curve proposed by Gardner and Ashraf (2006), which has been reported to provide accurate results for LDSS members under both tension and compression (Patton and Singh, 2012), was used. The Gardner and Ashraf model consists of, i) Ramberg-Osgood model (1943) up to 0.2% proof stress ($\sigma_{0.2}$), and ii) Gardner and Ashraf model from from $\sigma_{0.2}$ to $\sigma_{1.0}$ (see Eq. 1)

$$\varepsilon = \left(\frac{\sigma - \sigma_{0.2}}{E_{0.2}}\right) + \left(\varepsilon_{t1.0} - \varepsilon_{t0.2} - \frac{\sigma_{1.0} - \sigma_{0.2}}{E_{0.2}}\right) x \left(\frac{\sigma - \sigma_{0.2}}{\sigma_{1.0} - \sigma_{0.2}}\right)^{n'0.2,1.0} + \varepsilon_{t0.2} \tag{1}$$

where $\epsilon_{t1.0}$ and $\epsilon_{t0.2}$ are total strains at $\sigma_{1.0}$ (1% proof stress) and $\sigma_{0.2}$ (0.2% proof stress), respectively; and $n'_{0.2,1.0}$ is the strain hardening exponent. Although strength enhancement at the corner region due to cold working is expected (Ashraf *et al*., 2005), such consideration has been ignored in the current study. Hence, the results from the current FE models are likely to be on the lower side and thus conservative estimates of experimental values. Also, the effect of residual stresses in FE models are reported to be very small in the literature (e.g. Huang and Young, 2012, Ellobody and Young, 2005), and hence, the effect of residual stresses are not incorporated in the current study. The values of LDSS material parameters (Young's modulus, E, $\sigma_{0.2}$, $\sigma_{1.0}$, n and $n'_{0.2,1.0}$) used in the Gardner and Ashraf (2006)'s model are shown in Table 1 , for the specimens 80x80x4 and 60x60x3 (Theofanous and Gardner, 2009).

3 Validation of Finite Element Model

The FE models need to be validated with reliable experimental results to show that the modeling approach is acceptable and accurate. For the current study, in order to establish confidence and to validate the FE modelling approach, comparisons have been made with two experimental stub SHC (LDSS Square Hollow Column- 80x80x4 and 60x60x3) data from the work of Theofanous and Gardner (2009). The LDSS (Grade EN 1.4162) stress-strain material curves (derived based on Gardner and Ashraf model) for the two specimens are shown in Figs 3 and 4. These curves are first converted (see Eqs. 2-3) into their corresponding true-stress (σ_{true}) and true-plastic strain $\left(\varepsilon^{pl}_{true}\right)$ values and subsequently used as input to Abaqus.

$$\sigma_{true} = \sigma_{nom}(1 + \varepsilon_{nom}) \tag{2}$$

$$\varepsilon^{pl}{}_{true} = \ln(1 + \varepsilon_{nom}) - \frac{\sigma_{true}}{E_o} \tag{3}$$

where σ_{nom} and ε_{nom} are engineering stress and strain respectively. The geometrical dimensions of the two stub columns considered for validation are shown in Table 2. The results of validation is presented in the form of load (P) vs axial displacement (δ) in Fig. 5. From Fig. 5, it can be inferred that, the experimental variation of P vs δ are well captured by the present FE models, thereby showing the acceptability of the FE modelling approach adopted herein.

4 Parametric Study

The parametric study of LDSS flat oval stub columns has been performed by selecting non-compact (or slender) sections, based on the slenderness limit of $w/t \geq 40$ (see e.g. Zhu and Young, 2011). All the FE models comes under Class 4 ($l_f/t\varepsilon$ > 37; where $\varepsilon = \left(\frac{235}{f_y}\frac{E_o}{210000}\right)^{0.5}$, f_y is the material yield stress and E_o is the Young's modulus) section as per EN 1993-1-4 (2015). In total, 33 FE models have been analysed, specially noting ultimate load (P_u) and failure modes. The FE specimens are labelled following the nomenclature such as *l*150*w*300*r*150*t*3 where *l*150, *w*300, *r*150 and *t*3, denote flat length of 150 mm, width between flat elements of 300 mm, curve element radius of 150 mm and thickness of 3 mm, respectively. It may be mentioned that, although many design codes and manual are available for the design of cold formed stainless steel such as European (EN 1993-1-4, 2015) Code, American Society for Civil Engineers (ASCE 8-02, 2002) Standard, Australian/New Zealand Standard (AS/NZS 4673, 2001), Automotive Steel Design Manual (ASDM, 2002) etc. (hereafter referred to as 'codal/manual'), but none have been found to provide exclusively design provisions for structural flat oval hollow columns. However, it may be worth noting that ASDM (2002) provides design guidance i.e. consideration of effective areas, for elemental local buckling interaction of curve and flat panels, for general mechanical engineering applications. ASCE 8-02 (2002) and AS/NZS 4673 (2001) specifications are similar, with flat plate buckling coefficient k taken as 4 (Zhu and Young, 2012). Thus, in this study, predicted FE column strength are compared with the design strengths predicted by using EN 1993-1-4 (2015), AS/NZS 4673 (2001) or ASCE 8-02 (2002) and ASDM (2002) to check their applicability for non-compact (slender) LDSS flat oval hollow stub columns. Design consideration based on EN 1993-1-4 (2015), AS/NZS 4673 (2001) or ASCE 8-02 (2002) and ASDM (2002) are briefly described in the following section.

5 Design Considerations for EN 1993-1-4 (2015), AS/NZS 4673 (2001), ASCE 8-02 (2002) and ASDM (2002)

In this section, the design procedures based on EN 1993-1-4 (2015), AS/NZS 4673 (2001) or ASCE 8-02 (2002) and ASDM (2002) are described. As mentioned above, these codes are silent on the structural design of hollow steel members having flat oval cross sections (i.e. consisting of both curved and flat elements). Considering EN 1993-1-4 (2015), Class classification (for non-curved sections) is based on the cross-section slenderness ($l_f/t\varepsilon$), where, l_f is the flat element length (see Fig. 6 schematic representation of the effective length, l_{ef}): Class 1 ($l/t\varepsilon \leq 33$), Class 2 ($l_f/t\varepsilon \leq 35$), Class 3 ($l_f/t\varepsilon \leq 37$) and Class 4 ($l_f/t\varepsilon > 37$). In the calculation of column capacity, full or total area (A) of the cross section is considered for in Class 1,2,3 and the effective area (A_e) in case of Class 4 sections. It can be noted that, guidelines for the calculation of effective areas for curved elements are not suggested in the codes. However, Zhu and Young (2011, 2012) considered semicircular curved portion (of the flat oval section) to be fully effective (i.e. gross area of the semicircular curved section is considered for load calculation) as the local buckling resistance of curved portion is relatively higher than that of the flat plate. For the sections under consideration (with $w/t \geq 40$), all of them falls under Class 4.

5.1 EN 1993-1-4 (2015)

The column design strength of EN 1993-1-4 (2015) i.e. (P_{EN}) were estimated as per clause 5.2.3 of EN 1993-1-4 (2015). The flat plate effective width/length is given by Eq. (4):

$$l_e = \rho l_f \tag{4}$$

where, ρ is the effective width reduction factor calculated by Eq. (5) as shown below.

$$\rho = \frac{0.772}{\bar{\lambda}_p} - \frac{0.079}{\bar{\lambda}_p^{\,2}} \leq 1 \tag{5}$$

where, $\bar{\lambda}_p$ (element slenderness) is given by Eq. (6).

$$\bar{\lambda}_p = \frac{l_f / t}{28.4\varepsilon\sqrt{k}} \tag{6}$$

The effective area expression of flat oval column is calculated by Eq. (7) see Fig. 6(a).

$$A_e = A_g - 2\,(l_f - l_{ef})t \tag{7}$$

The cross-sectional resistance as per EN 1993-1-4 (2015) is then given by Eq. (8).

$$P_{EN} = f_y A_e \tag{8}$$

where, A = A_g or A_e (i.e. gross or effective area) depending on cross sectional class type.

5.2 AS/NZS 4673 (2001) and ASCE 8-02 (2002)

As per AS/NZS 4673 (2001) and ASCE 8-02 (2002), the member capacity is computed based on the effective width given by Eqs 9-10. The effective width (l_{ef}) is dependent on the value of cross-sectional slenderness ratio, λ.

For $\lambda \leq 0.673$, $l_{ef} = l_f$ (9)

For $\lambda > 0.673$, $l_{ef} = \rho l_f$, (10)

$$\text{where, } \rho = \frac{\left(1 - \frac{0.22}{\lambda}\right)}{\lambda} \leq 1.0\,;\ \lambda = \left(\frac{1.052}{\sqrt{k}}\right)\left(\frac{l_f}{t}\right)\left(\sqrt{\frac{f}{E}}\right)$$

where f ($= \sigma_{cr}$) is the critical stress for unstiffened compression element. The value of k is conservatively taken as 4.0. The member capacity is then computed as per Eq. (11).

P_{ASCE} or $P_{AS/NZS} = f_y A_e$; where A_e is calculated based on Eq. (7) see Fig. 6a. (11)

5.3 ASDM (2002)

In the case of ASDM (2002), the total effective area is calculated as a sum of the effective areas of flat and curved sections (see Fig. 6b). The effective width of flat (l_{ef}) and curved (l_{ec}) elements are determined as a function of cross-sectional slenderness ratio (λ) using Eqs. 9 and 10 (AS/NZS 4673, 2001; Zhu and Young, 2011). However, as f_y > 552 MPa, a reduced yield strength (f_{yrs}) be substituted for limiting value of f (ASDM, 2002) as given by Eq. 12.

$$f_{yrs} = f = \left(1 - 0.2\sqrt{\frac{l_f}{t}}\sqrt{\frac{f_y}{E}}\right) f_y \tag{12}$$

Further, for the curve portion instead of completely neglecting the central portion as done for flat elements, an effective thickness (t_e) has been considered (Eq. 13).

$$t_e = \left(\frac{A_o}{A}\right)\left(\frac{f_y}{f}\right) t \tag{13}$$

where, A_o denotes the equivalent area in compression element respectively (see Eqs. (14-16))

$$A_o = A\,; \qquad \text{for} \quad \frac{D}{t} \leq 0.114\frac{E}{f_y} \tag{14}$$

$$A_o = \left(\frac{2}{3} + \frac{0.038\frac{E}{f_y}}{\frac{D}{t}}\right) A \qquad \text{for} \quad 0.114\frac{E}{f_y} < \frac{D}{t} \leq 0.448\frac{E}{f_y} \tag{15}$$

$$A_o = \left(\frac{0.336\frac{E}{F_y}}{\frac{D}{t}}\right) A \qquad \text{for} \quad \frac{D}{t} \geq 0.448\frac{E}{F_y} \tag{16}$$

where, D = diameter of the curve element.

As seen in Eq, (14), the whole curved portion is taken as effective for $D/t \leq 34.22$ based on the value of E = 197200 N/mm^2 and f_y = 657 N/mm^2.

Then, the effective area for the curved (A_{ec}) and flat (A_{ef}) portions are calculated as per Eqs. (17-18). The total effective area of the flat oval section (A_e) as per ASDM (2002) is then given by Eq. 19.

$$A_{ec} = 2(l_c - l_{ec})t_e + 2tl_{ec} \tag{17}$$

$$A_{ef} = 2tl_{ef} \tag{18}$$

$$A_e = A_{ec} + A_{ef} \tag{19}$$

where, l_c is the arc length of the curve element.

The member capacity of ASDM (2002) is calculated as per Eq. 20.

$$P_{ASDM} = f_y A_e \tag{20}$$

In ASDM, the ineffective portion of the curve element is assumed to carry critical buckling stress (unlike a flat element) of a circular cylinder with equivalent radius and thickness (ASDM, 2002; Zhu and Young, 2012).

6 Reliability Analysis

The present FE results of flat-oval hollow stub columns have been compared with those predicted by various international standards or codes (e.g. EN 1993-1-4, 2015; ASCE 8-02, 2002; AS/NZS 4673, 2001), design manual (e.g. ASDM, 2002),), in order to examine their appropriateness. Based on the FE and codal comparisons, reliability analysis has been performed following the ASCE method (ASCE 8-02, 2002) for cold formed steel structures, in order to evaluate the reliability of using the aforementioned design codes /manual for the design of LDSS flat-oval stub columns. In the reliability analyses, the resistance factor (Φ) of 0.91, 0.85, 0.85 are used for the EN 1993-1-4 (2015), ASCE 8-02 (2002) and AS/NZS 4673 (2001) specifications, respectively, have been used to find the reliability index (β). For ASDM(2002), the resistance factor (Φ) of 0.85 has been adopted as in the work of Zhu and Young (2011).

The load combinations of 1.35DL+1.5LL, 1.2DL+1.6LL and 1.25DL+1.5LL (where LL and DL are the live and dead loads) have been used for the reliability analysis for EN 1993-1-4 (2015), ASCE 8-02 (2002) and AS/NZS 4673 (2001) respectively. The ratio of DL/LL is taken as 0.2 as per NAS (2007). The statistical values of M_m, F_m, V_M and V_F (i.e. mean, coefficients of variation (COV) of material and fabrication, respectively) are taken as 1.10, 1.0, 0.10 and 0.05 according to the ASCE specification (ASCE 8-02, 2002). For the case of ASDM (2002) also, following Zhu and Young (2011), the load combination has been taken as 1.2DL+1.6LL, which is similar to that given by ASCE 8-02 (2002). In order to take into account of the influence of the number of data, a correction factor (C_p) given in Equation F1.1-3 of NAS (2007) specification has been considered. From NAS (2007), a target reliability index (β_o) value of 2.5 is used for the reliability analyses. This value defines the lower limit for a design to be considered reliable.

7 Results and discussions

The FE results of the flat oval LDSS hollow stub columns under axial compression have been presented in the form of deformation or failure modes, followed by the effect of cross-sectional parameters like r, l_f, and t, on P_u (i.e. load capacity). Then, the FE results are compared with predictions from EN 1993-1-4 (2015), AS/NZS 4673 (2001), ASCE 8-02 (2002), ASDM (2002) to check their applicability for flat-oval LDSS hollow slender columns. The results are presented in the following sections.

7.1 Deformation shapes

Von-Mises stress contours superimposed on deformed shape for *l*300*w*300*r*300*t*3 specimen (i.e. l_f = 300 mm, w = 300 mm, r = 300 mm) corresponding to δ_u (axial deformation/shortening corresponding to ultimate load, P_u) and 1.5δ_u (i.e. 1.5 times the axial deformations at P_u) for Class 4 (t = 3 mm; slender or non-compact cross-section; w/t $\geq$ 40) section are shown in Fig. 7. In Fig. 7, the values of von-Mises stress $\geq$ 657 MPa (i.e. $\sigma_{0.2}$) are colored in grey, in order to identify areas which have crossed the yield stress. This method is followed in all the subsequent such contour plots. In Fig. 7a, initiation of local buckling is visible on the flat surfaces (or elements) with very small areas at the junction of flat and curve surfaces showing signs of yielding. Although initiation of buckling is not readily seen at P_u, evidences of non-uniform distribution of stresses can be seen on the curve surfaces (see Fig. 7a). At post-buckling load at 1.5δ_u, buckling on both the flat and curve surfaces can be observed along with extended areas of yielded zones, especially corner region and central portion of the curve surfaces (Fig. 7b). From Figs. 7a and 7b, it can also be seen that as compared to the flat surfaces, relatively more surface areas (i.e. effective in taking load) of higher stress is observed on curve surface. Presence of effective areas (i.e. relatively effective in carrying load) on the sides (shown by relatively higher stress regions on the sides of the flat surface) and ineffective areas in the central portion of the flat surface can also be seen in Fig. 7a. Further, evidence of interaction between the flat and curve elements can be seen for thin section (see yielded zones at the junction of flat and elements in Figs. 7a and 7b).

7.2 Effect of curvature radius (r)

Variation of load (P) with axial shortening/deformation (δ) for the selender (t = 3 mm) section stub columns, for r = 150, 300 and 750 mm (l_f = 300 mm) are shown in Fig. 8. It can be seen that as the value of r increases there is a drop in the values of P_u. For the semicircular section (i.e. r = 150 mm or r/w = 0.5), post P_u, snap-through buckling pattern can be seen, where at P_u (T1), initiation of bucking can be seen on the flat face (i.e. not on the surface) with the appearance of a small yielded portion located at the junction of plate and surfaces around mid-height. It is observed that, the semi-circular section give the highest P_u. Following the drop in P_u due to buckling at the mid-height of the flat portion (T2), a somewhat stable load profile can be seen till around T3 (T3 corresponds to the second peak), and this may be related to the redistribution of the load towards the curve portions. At post P_u (i.e. T2 and T3), an increase in the spread of high stress or yielded region can be observed on the surfaces, indicating a major portion of the load is carried by the curve section, due to enhanced stiffness of the curve section. Post T3 drop in P, may then be related to the enhanced buckling of the flat portions at column mid-height, with stress relaxation and redistribution in the curve portions (see T4).

On the other hand, for larger values of r (or flatter curve sections), a snap-back buckling pattern is observed, where at P_u, initiation of buckling can be seen both on the flat and curve sections (S1), with the occurrence of a very small yielded portion located at the mid-height of the curve section. However, it can be seen from S2, that snap-back buckling has taken place due to the occurrence of buckling at the mid-height (with sudden relaxation of stress on either sides of the mid-height region) of the curve portion. Beyond S2, P increases till around S3 (S3 corresponds to the second peak), and this occurs mainly because of the increase in yielded zone (indicating more load being taken up) near the mid-height column of the curve portion. Again it must be noted that the spread of this yielded zone towards the curve portion is constrained due to the relatively sharp junction corner, hence confined to the junction areas.

At post P_u, the yielded region on the curve surface is increased and spread to the junction between flat and curve surfaces (S2 and S3). Also, it is seen that deformation at P_u (i.e. δ_u) decreases with reducing r/w value, suggesting that semicircular section provided improved ductility at P_u, as compared to other flatter sections. In contrast to semi-circular curve sections, post P_u yielded region is confined to a relatively smaller region at mid-height, indicative of lesser load bearing capacity of the flatter sections. The drop in P beyond S3, may be associated with the buckling of the flat portions (see S4) of the column, with the yielded zone being increased on both the curve and flat portions.

Further, for the section under consideration (t = 3 mm), there is an indication of the tendency to spread the buckling from flat elements on to the curve elements, at lower r values e.g. r = 150 mm (T1, T2 and T3), although such spread appears to be absent for larger r values (say r = 750 mm; S1, S2, S3). Such spreading phenomena for small values of r/t have been reported by Parks and Yu (1989) in their stiffened flat-oval experimental tests. This may be because, when the radius of the curve portion is small and the flat length is sufficiently long, buckling of the flat element would have occurred earlier, and the chance of spreading the flat buckling would be sufficiently improved when a smooth corner junction / transition of the flat and elements is present. When the radius of the curve portion is large, there would be a relatively sharp corner at the junction of the flat and curve elements, which would arrest the flat element buckling from crossing over to the curve elements.

7.3 Effect of flat length (l_f)

In the previous plots (Fig. 8), it has been observed that the maximum value of load capacity (P_u) is obtained when semicircular sections are used (keeping flat length, l_f constant) on the sides of flat plate portions, hence in order to ascertain the effects of length of the flat portion, results are presented keeping r/w = 0.5 or r = 150 mm, for various values of l_f = 300 – 700 mm. Fig. 9 shows the variation of P with δ for slender (t = 3 mm) section, for l_f = 300, 400 and 600 mm. It can be seen from Fig. 9 that, snap through buckling behaviour is observed, with very mild variation in the pattern and increase in the values of P_u. As stated before, at P_u buckling of the flat is initiated, with most of the post P_u load being carried (identified by relatively higher stressed region) by the semicircular portions (S2, S3 and S4). The spread of flat section buckling on to the curve section can be seen for values of l_f = 300 to 600 mm (S2, S3, and S4), indicating that for the slender sections, flat section buckling controls the column strength. The value of δ_u remains almost unaffected for increasing values of l_f.

7.4 Comparison of FE and design strength results

Comparison of FE and codal/manual (EN 1993-1-4, AS/NZS 4673, ASCE 8-02, and ASDM) values of P_u for different r values are shown in Fig. 10, for t = 4 (l_f = 300 mm). The FE results are lower than the codal results, showing the unconservative nature of the codes for thin sections. In Fig. 11, comparison between FE and codal predictions of P_u are plotted for two values of r (r = 150 mm and r = 750 mm), for thicknesses, t = 3-7.5 mm. It can be seen from Fig. 11 that for the thinner/slender sections ($t \leq 7.5$ mm), FE predicted lower values of P_u;. Thus it can be inferred that for thinner/slender sections (for a constant flat length), codal predictions are unconservative. Similar comparisons of FE and codal P_u predictions are plotted in Fig. 12 for different values of l_f, for t = 4 mm, keeping r constant at 150 mm (i.e. semicircular section). Like the previous observation for constant l_f (i.e. varying r), in the case of constant r (i.e. varying l_f), it can be seen that, FE predictions are lower for thinner sections as compared to that of codal predictions as shown in Fig. 13.

The column strengths calculated by FE (P_{FE}) analysis have been compared with the values calculated on the basis of the design codes of EN 1993-1-4 (P_{EN}), AS/NZS 4673 standard ($P_{AS/NZS}$), ASCE 8-02 (P_{ASCE}), ASDM (P_{ASDM}) in Table 3.

The comparisons are plotted in the form of normalised load ratios *viz.*, $P_{FE}/P_{AS/NZS}$, P_{FE}/P_{ASCE}, P_{FE}/P_{EN}, P_{FE}/P_{ASDM}. It can be seen from Table 3, that, the values of mean; COV and reliability index (β) are 0.88, 0.84, 0.84, 0.94; 0.18, 0.17, 0.17, 0.15; 1.44, 1.50, 1.67, 2.14 respectively, for P_{FE}/P_{EN}, $P_{FE}/P_{AS/NZS}$, P_{FE}/P_{ASCE}, P_{FE}/P_{ASDM}. The value of β provided by EN 1993-1-4, AS/NZS 4673, ASCE 8-02 and ASDM are found to be less than 2.5 (target value), suggesting that EN 1993-1-4, AS/NZS 4673, ASCE 8-02, and ASDM design rules are unconservative for the design of non-compact flat oval stub column sections and further study has been done to suggest some modification in the current design rules and manuals.

8 Proposed modifications to EN 1993-1-4, AS/NZS 4673/ ASCE 8-02 and ASDM for flat oval section

As discussed above in Section 7.4 (also see Table 3), for non-compact (or slender) flat oval sections (i.e. for $w/t \geq 40$), the predictions made by AS/NZS 4673, ASCE 8-02, EN 1993-1-4 and ASDM are found to be unreliable with $\beta < 2.5$. Hence, following the approach adopted by ASDM for combined curve and flat sections (see Parks and Yu, 1987), further modification to the effective thickness (t_e see Section 5.3) in order to arrive at suitable effective area values, so that the predictions become reliable. This has been attempted by incorporating a thickness reduction factor (TRF) to the expression of t_e as shown in Eq. (21).

$$t_e = TRF\left(\frac{A_o}{A}\right)\left(\frac{F_y}{f}\right)t \tag{21}$$

In order to arrive at an optimal value of TRF, the value of TRF has been varied from 0.3-1.0, and corresponding β value has been estimated for EN 1993-1-4(2015), AS/NZS 4673(2001), ASCE 8-02 and ASDM (2002) predictions of load capacity. The computed variation of β with TRF is plotted in Fig. 14 (see also Table 4). It can be observed that, values of TRF in the range ~0.5-0.6 are able to provide the required target value of β_o (i.e. 2.5). Hence, a conservative value of TRF = 0.5 has been deduced for further modification to t_e. The proposed expression for t_e (or t_{ep}) has becomes Eq. (22).

$$t_{ep} = 0.5\left(\frac{A_o}{A}\right)\left(\frac{F_y}{f}\right)t \tag{22}$$

The new expression for the effective area of the curve portion (A_{ec}) is then given by Eq. 23.

$$A_{ec} = 2(l_c - l_{ec})t_{ep} + 2tl_{ec} \tag{23}$$

Following the procedures outlined in above Section 5 (EN 1993-1-4 (2015), AS/NZS 4673 (2001), ASCE 8-02(2002), ASDM (2002) in conjunction with Eq. 23 (see Fig. 6(c)), the results of (proposed) modified EN 1993-1-4(2015), AS/NZS 4673(2001), ASCE 8-02 (2002) and ASDM (2002) predictions of load capacity are then compared with those of FE results ($w/t \geq 40$) in Table 3 and Fig. 15. In Table 3, $P_{EN(p)}$, $P_{AS/NZS(p)}$, $P_{ASCE(P)}$ and $P_{ASDM(p)}$ corresponds to the load capacity predicted by the proposed EN 1993-1-4(2015), AS/NZS 4673(2001), ASCE 8-02 (2002) and ASDM (2002) expressions, respectively. It can be readily seen that, with the adoption of the proposed effective thickness expressions (see Eqs. 22 and 23), the value of β has exceeded the target value of 2.5 (i.e. β = 2.77, 2.66, 2.84 and 2.98 for the proposed EN 1993-1-4(2015), AS/NZS 4673(2001), ASCE 8-02(2002) and ASDM (2002) expressions). Fig. 15 shows some comparison of FE and (proposed) modified EN 1993-1-4(2015), AS/NZS 4673(2001), ASCE 8-02 (2002) and ASDM (i.e. EN 1993-1-4$_{(p)}$, $P_{AS/NZS(p)}$, $P_{ASCE(P)}$ and ASDM$_{(P)}$ predictions), for increasing values of section thickness (t), for r = 150 and 450 (see Fig. 15(a,b))and l_f = 500 and 600 (see Fig. 15(c,d)). The conservativeness of the proposed predictions can be seen from Table 3.

9 Conclusions

Parametric study of the structural behaviour of fixed ended LDSS flat oval section stub columns, by varying l_f(flat element length), r (radius of curved element), t (thickness), keeping w (spacing between flat elements) and h (height of column) constant at 300 mm and 900 mm respectively, using the commercial finite element software, Abaqus, is presented. Based on the FE analyses, the following conclusions have been obtained:

LDSS flat oval sections with semicircular elements on either sides of the flat elements (i.e. r/w = 0.5) provided the maximum column strength (P_u), with increasing P_u for increasing l_f/w.

EN 1993-1-4, AS/NZS 4673, ASCE 8-02, and ASDM design rules are unconservative for the design of non-compact LDSS flat oval stub column sections

An expression has been proposed for calculating the effective thickness of curve elements of flat oval LDSS sections with $w/t \geq 40$, which can provide reliable load capacity predictions when used with EN 1993-1-4 (2015), AS/NZS 4673 (2001), ASCE 8-02 (2002) and ASDM (2002) equations.

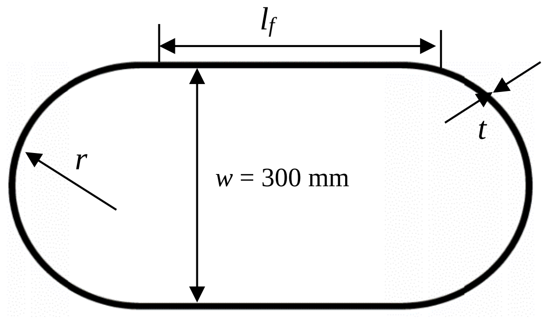

Fig. 1 Flat oval hollow section.

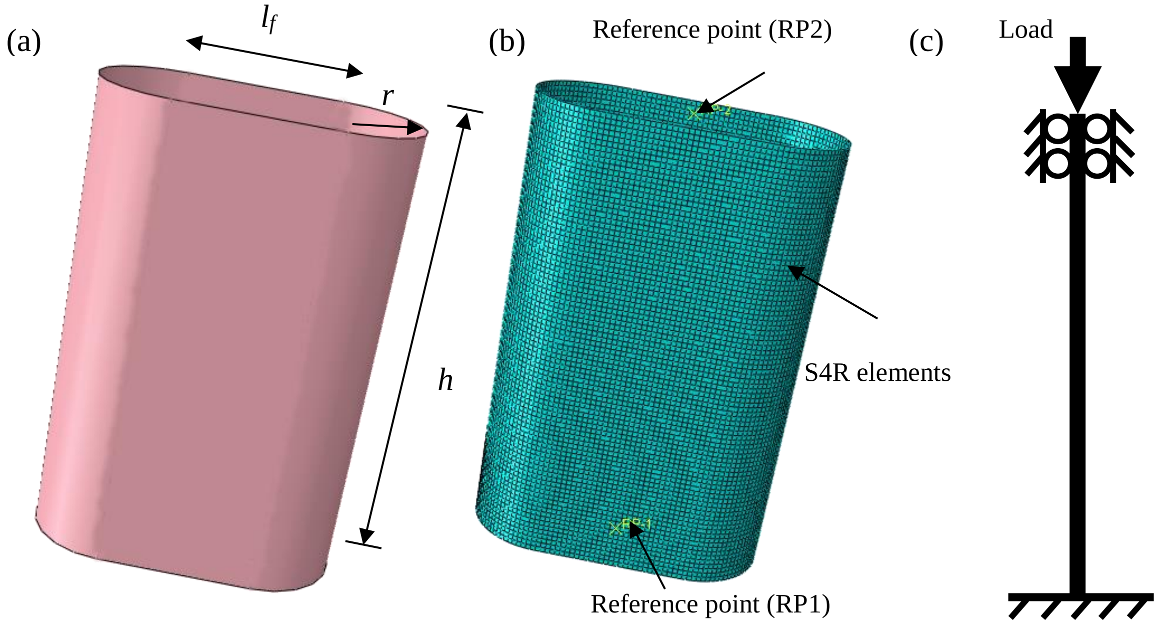

Fig. 2 Typical FE (a) geometry, (b) FE mesh, (c) boundary conditions of LDSS flat oval hollow column.

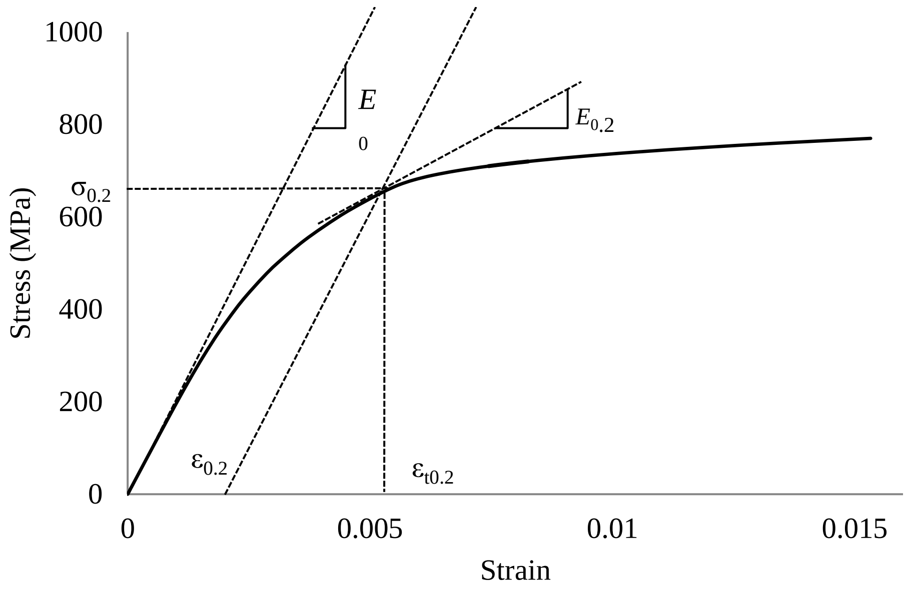

Fig. 3 **Experimental stress-strain curve of LDSS material Grade EN 1.4162 for 80x80x4 (Theofanous & Gardner,2009).**

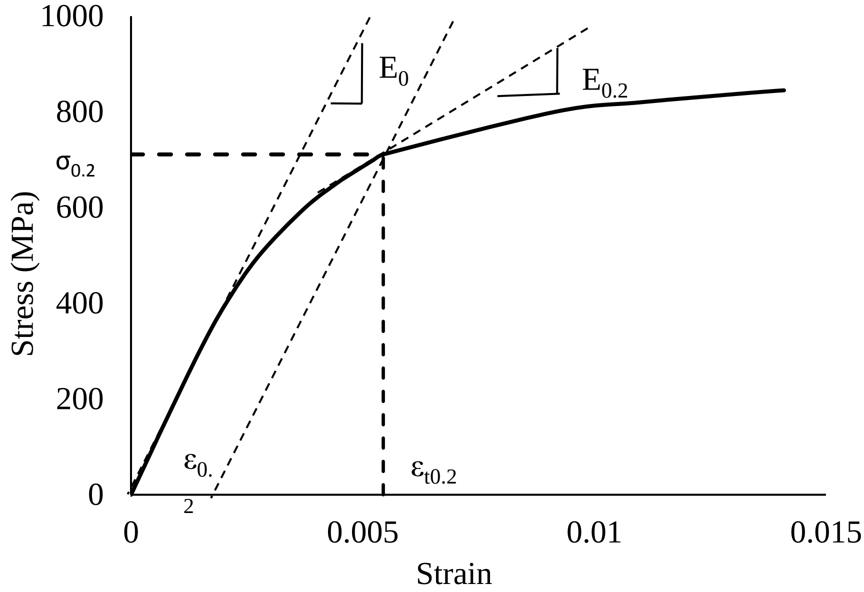

Fig. 4 **Experimental stress-strain curve of LDSS material Grade EN 1.4162 for 60x60x3 (Theofanous & Gardner, 2009).**

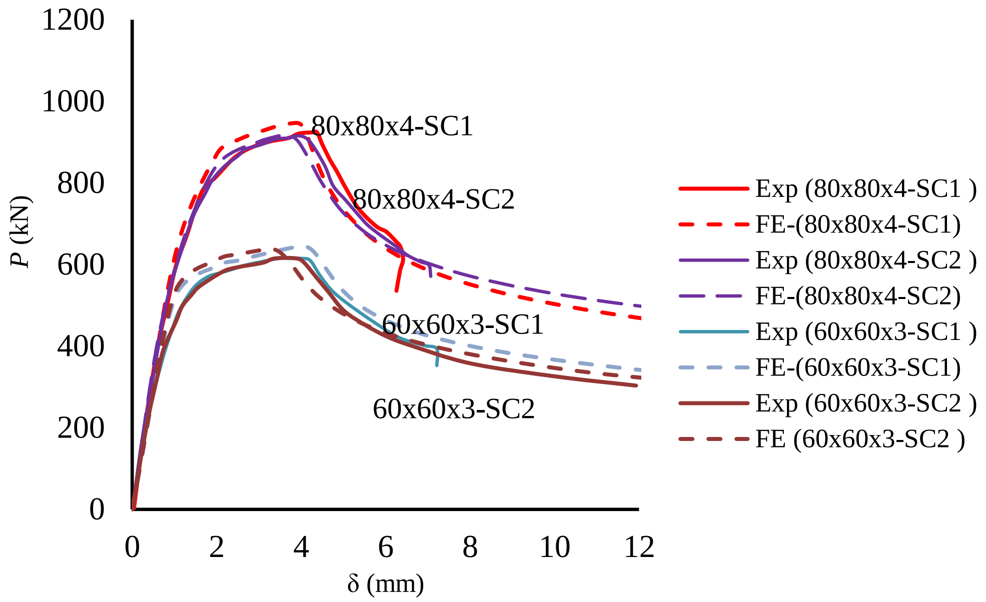

Fig. 5 **Comparison of experimental (Theofanous and Gardner, 2009) and FE results of load (*P*) vs axial displacement (*δ*).**

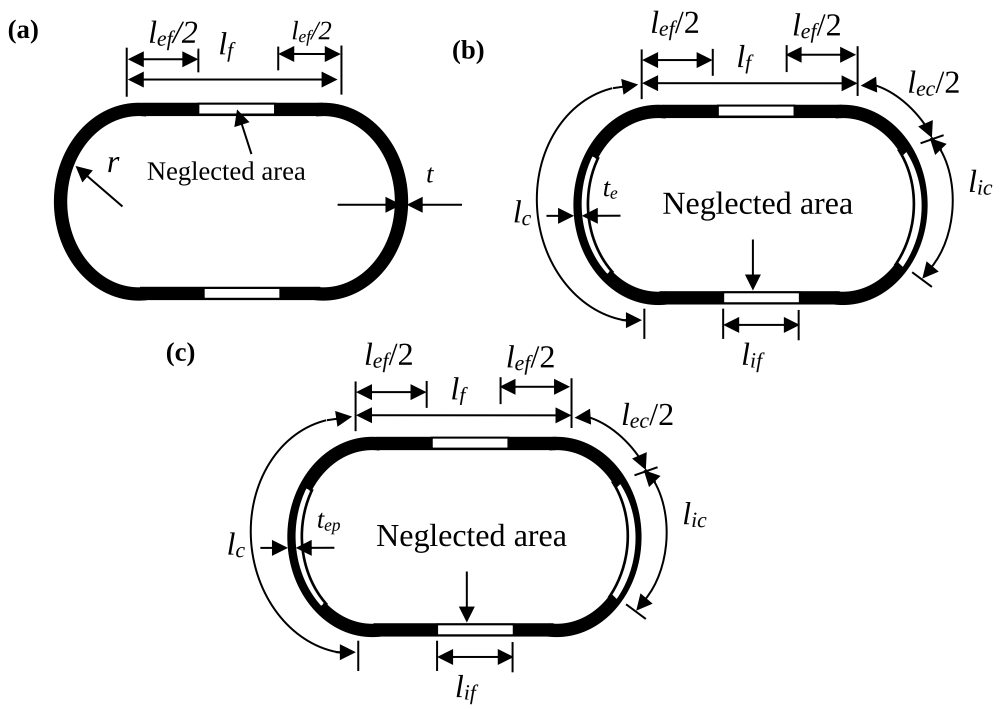

Fig. 6 **Schematic representation of area deductions: (a) AS/NZS 4673 (2001)/ASCE 8-02 (2002), EN 1993-1-4 (2015), (b) ASDM (2002) and (c) Proposed modified EN 1993-1-4(p), AS/NZS 4673(p), ASCE 8-02(p), and ASDM(p)**

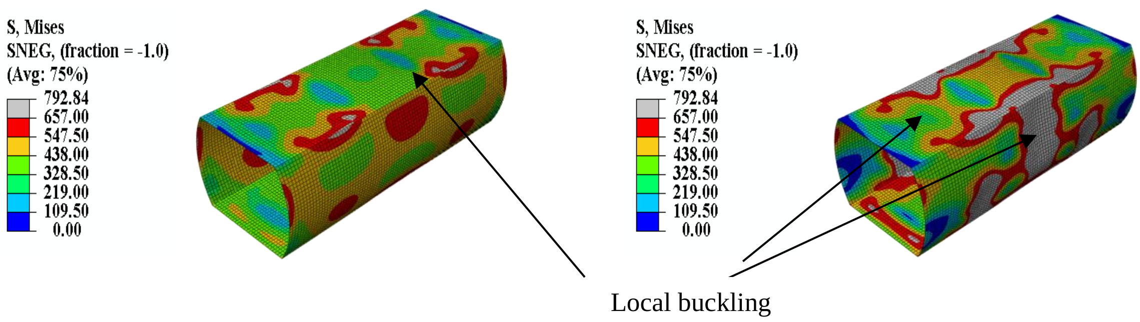

(a) at δ_u (b) at 1.5 δ_u

g. h.

Fig. 7 **Typical Von-Mises stress (superimposed on deformed shape: a) at ultimate load displacement (δ_u) and b) 1.5 δ_u (l_f = 300 mm; r = 300 mm, t = 3 mm).**

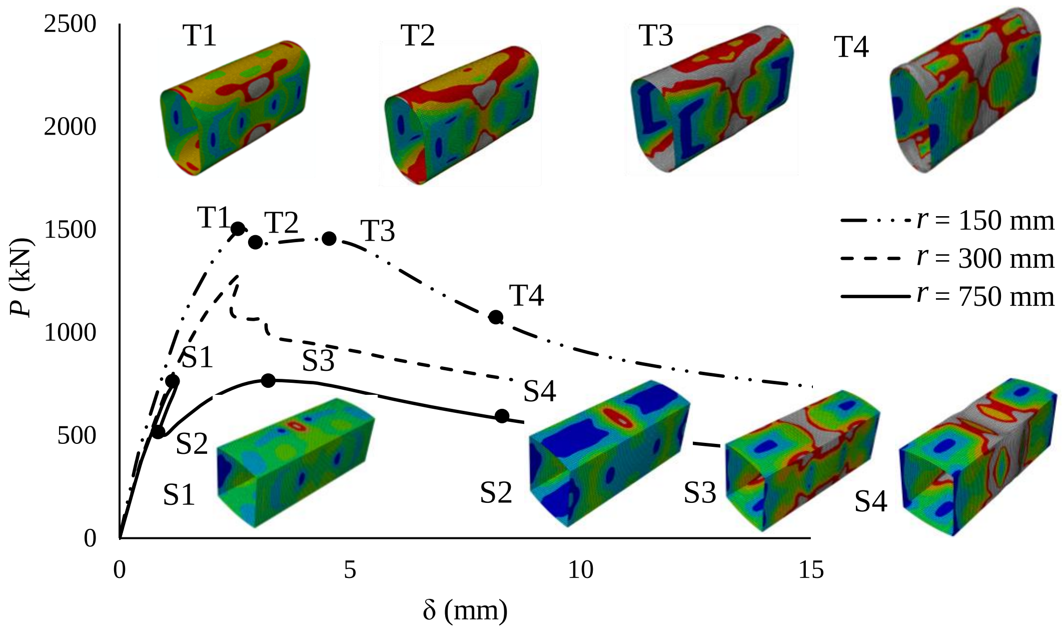

Fig. 8 **Variation of P with δ (l_f = 300 mm, t = 3.0 mm).**

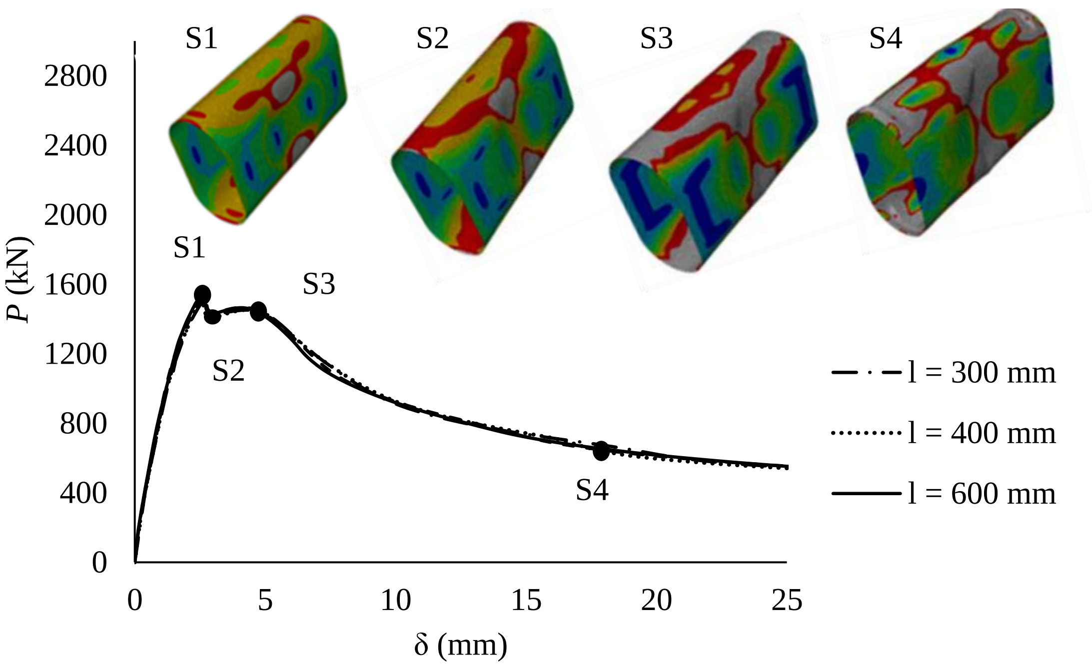

Fig. 9 **Variation of P with δ (r = 150 mm, t = 3 mm).**

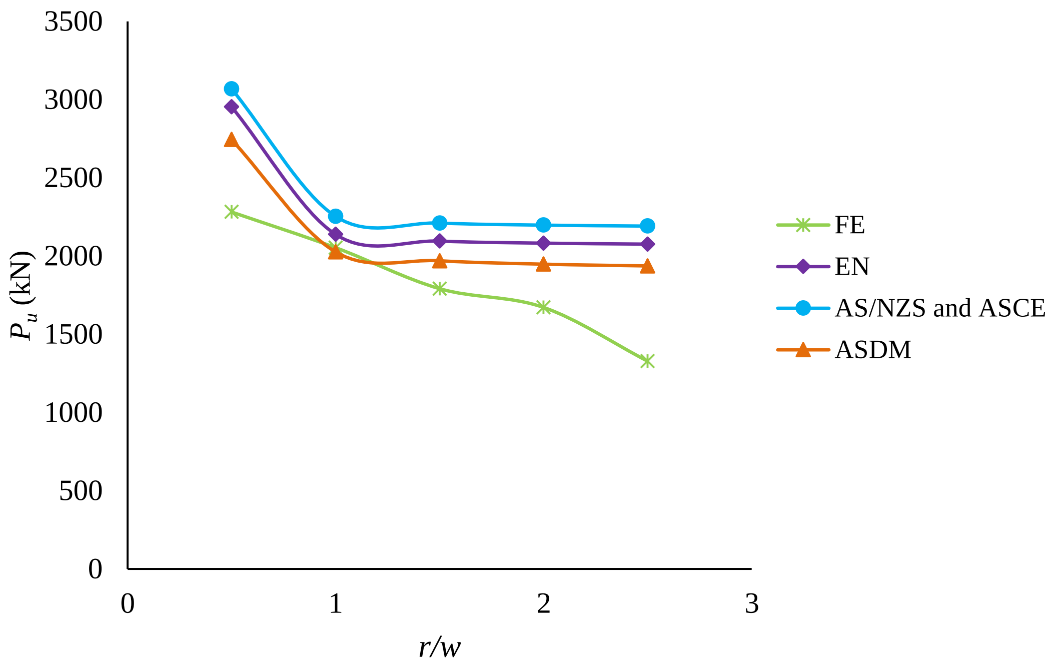

Fig. 10 Comparison of FE and codal predictions of P_u (l_f = 300 mm, t = 4 mm).

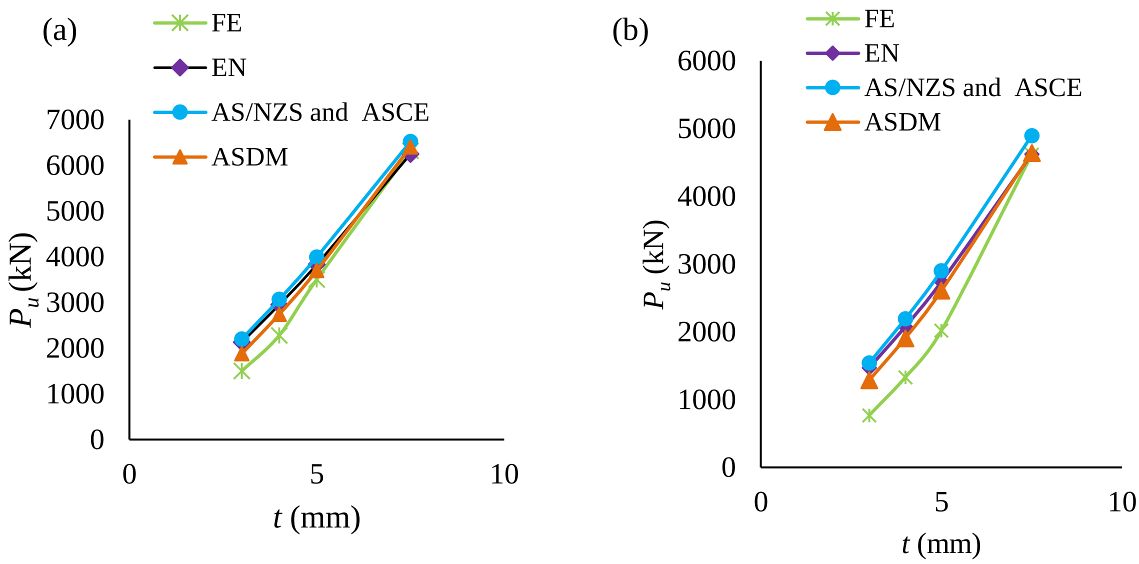

Fig. 11 Comparison of FE and codal predictions of P_u: a) r = 150 mm, and b) r = 750 mm (l_f = 300 mm).

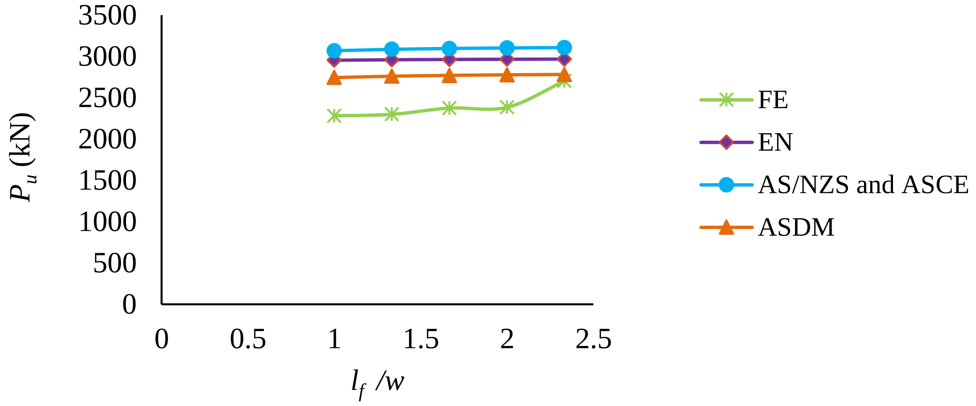

Fig. 12 Comparison of FE and codal predictions of P_u (r = 150 mm, t = 4 mm).

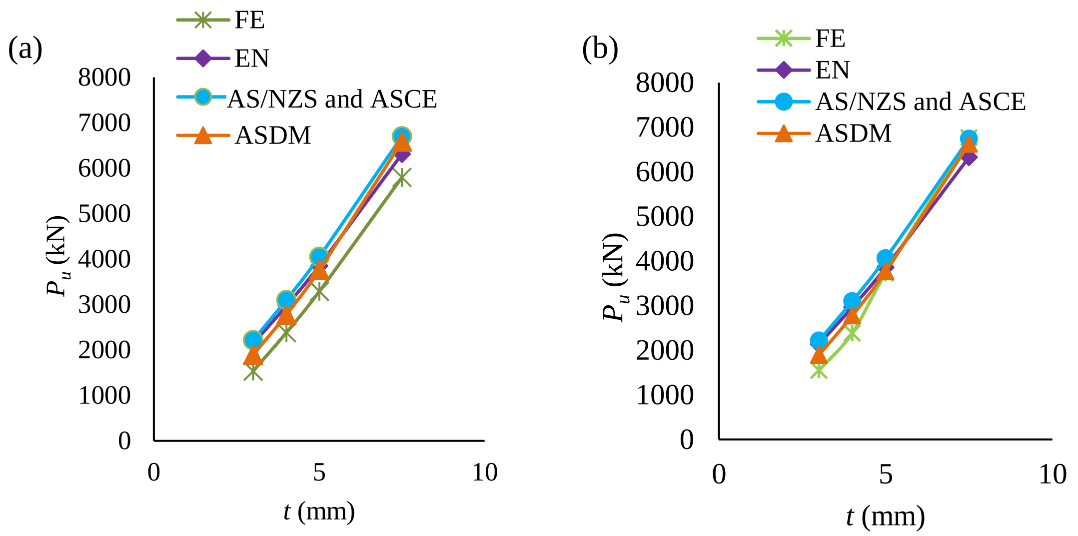

Fig. 13 Comparison of FE and codal predictions of P_u: a) l_f = 500 mm and b) l_f = 600 mm (r = 150 mm).

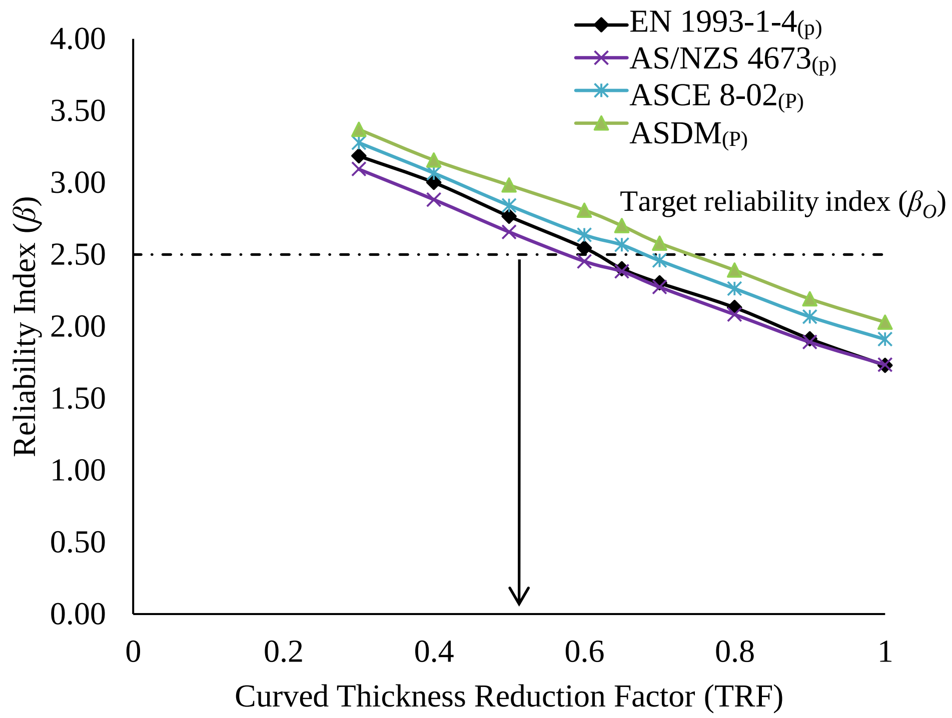

Fig. 14 Reliability index (β) vs TRF (curved Thickness Reduction Factor) for (proposed) modified design codes.

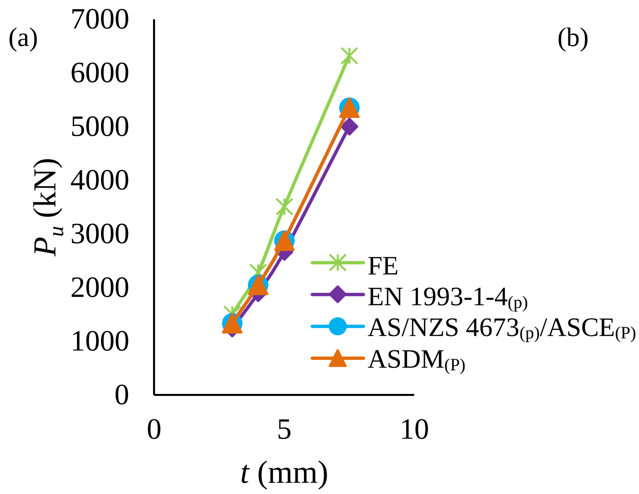

(a) *l*300*w*300*r*150

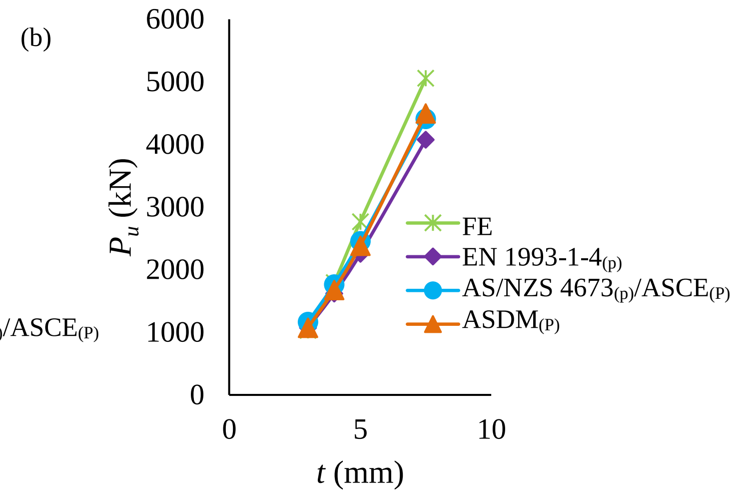

(b) *l*300*w*300*r*450

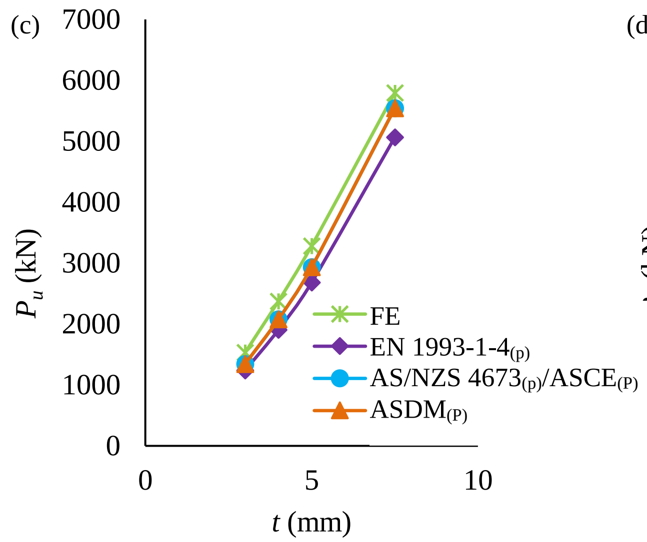

(c) *l*500*w*300*r*150

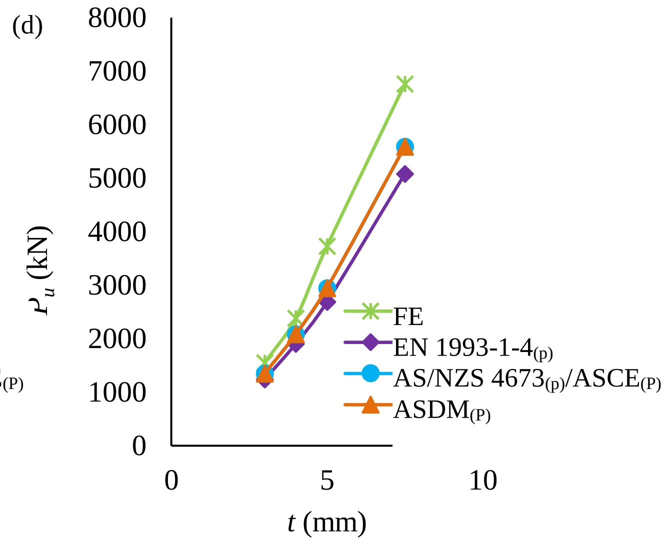

(d) *l*600*w*300*r*150

Fig. 15 Comparison of FE and (proposed) modified codes (EN 1993-1-4$_{(P)}$, AS/NZS 4673$_{(P)}$ or ASCE 8-02$_{(P)}$, ASDM$_{(P)}$).

Table 1 Compressive LDSS flat material properties (Theofanous and Gardner, 2009).

Cross-section	*E* (MPa)	$\sigma_{0.2}$ (MPa)	$\sigma_{1.0}$ (MPa)	Compound R-O coefficients	
				n	$n'_{0.2,1.0}$
80x80x4	197200	657	770	4.7	2.6
60x60x3	206400	711	845	5.0	2.7

Table 2 Stub column dimensions (Theofanous and Gardner, 2009).

Specimen	*L* (mm)	*B* (mm)	*h* (mm)	*t* (mm)	r_i (mm)
80x80x4-SC1	319.7	80	80.5	3.88	3.8
80x80x4-SC2	332.2	80	80	3.81	3.6
60x60x3-SC1	239.8	60	60	3.09	2.3
60x60x3-SC2	240.0	60	60	3.17	2.1

L = Length, B = Width, h = height, t = thickness, r_i = internal corner radius

Table 3 Comparison of design strengths with FE strengths (w/t ≥ 40).

Specimen	Current codes				Proposed modified codes			
	$\frac{P_{FEA}}{P_{EN}}$	$\frac{P_{FEA}}{P_{AS/NZS}}$	$\frac{P_{FEA}}{P_{ASCE}}$	$\frac{P_{FEA}}{P_{ASDM}}$	$\frac{P_{FEA}}{P_{EN\ (p)}}$	$\frac{P_{FEA}}{P_{AS/NZS\,(p)}}$	$\frac{P_{FEA}}{P_{ASCE(p)}}$	$\frac{P_{FEA}}{P_{ASDM\ (p)}}$
l300w300r150t3	0.70	0.68	0.68	0.79	1.21	1.13	1.13	1.13
l300w300r150t4	0.77	0.74	0.74	0.82	1.20	1.11	1.11	1.11
l300w300r150t5	0.91	0.87	0.87	0.94	1.32	1.22	1.22	1.22
l300w300r150t7.5	1.01	0.97	0.97	0.98	1.26	1.18	1.18	1.18
l300w300r300t3	0.84	0.80	0.80	0.93	1.18	1.09	1.09	1.18
l300w300r300t4	0.96	0.91	0.91	1.01	1.25	1.15	1.15	1.21
l300w300r300t5	1.04	0.98	0.98	1.06	1.37	1.25	1.25	1.22
l300w300r300t7.5	1.12	1.06	1.06	1.09	1.29	1.19	1.19	1.17
l300w300r450t3	0.69	0.66	0.66	0.77	0.96	0.89	0.89	0.96
l300w300r450t4	0.85	0.81	0.81	0.91	1.11	1.02	1.02	1.07
l300w300r450t5	1.00	0.94	0.94	1.03	1.23	1.13	1.13	1.16
l300w300r450t7.5	1.09	1.02	1.02	1.06	1.24	1.15	1.15	1.12
l300w300r600t5	0.96	0.91	0.91	0.99	1.18	1.08	1.08	1.12
l300w300r600t7.5	1.04	0.98	0.98	1.02	1.16	1.07	1.07	1.08

l300w300r750t3	0.52	0.50	0.50	0.59	0.72	0.67	0.67	0.72
l300w300r750t4	0.64	0.61	0.61	0.69	0.83	0.76	0.76	0.80
l300w300r750t5	0.74	0.69	0.69	0.84	0.99	0.91	0.91	0.94
l300w300r750t7.5	1.00	0.94	0.94	0.98	1.11	1.03	1.03	1.03
l400w300r150t3	0.70	0.69	0.69	1.05	1.21	1.12	1.12	1.12
l400w300r150t4	0.78	0.75	0.75	1.08	1.21	1.11	1.11	1.11
l400w300r150t5	0.84	0.80	0.80	1.12	1.21	1.11	1.11	1.11
l400w300r150t7.5	1.11	1.05	1.05	1.35	1.38	1.27	1.27	1.27
l500w300r150t3	0.72	0.69	0.69	0.80	1.24	1.14	1.14	1.14
l500w300r150t4	0.80	0.77	0.77	0.84	1.25	1.14	1.14	1.14
l500w300r150t5	0.85	0.81	0.81	0.86	1.22	1.12	1.12	1.12
l500w300r150t7.5	0.92	0.86	0.86	0.87	1.14	1.05	1.05	1.05
l600w300r150t3	0.73	0.70	0.70	0.80	1.25	1.15	1.15	1.15
l600w300r150t4	0.80	0.77	0.77	0.84	1.25	1.14	1.14	1.14
l600w300r150t5	0.97	0.91	0.91	0.97	1.39	1.26	1.26	1.26
l600w300r150t7.5	1.07	1.00	1.00	1.00	1.33	1.21	1.21	1.21
l700w300r150t4	0.91	0.87	0.87	0.95	1.42	1.29	1.29	1.29
l700w300r150t5	1.00	0.94	0.94	1.00	1.43	1.30	1.30	1.30
l700w300r150t7.5	1.11	1.02	1.02	1.04	1.38	1.25	1.25	1.25
Mean (P_m)	0.88	0.84	0.84	0.94	1.21	1.11	1.11	1.12
COV (V_p)	0.18	0.17	0.17	0.15	0.13	0.13	0.13	0.11
Reliability index (β)	1.44	1.50	1.67	2.14	2.77	2.66	2.84	2.98

Table 4 Variation of reliability index (β) with curve thickness reduction factor (TRF).

No. of samples	**Curved Thickness Reduction Factor, TRF**	β **(EN 1993-1-4$_{(P)}$)**	β **(AS/NZS 4673$_{(P)}$)**	β **(ASCE 8-02$_{(P)}$)**	β **(ASDM$_{(P)}$)**
33	0.30	3.19	3.09	3.28	3.37
33	0.40	3.00	2.88	3.07	3.16
33	0.50	2.77	2.66	2.84	2.98
33	0.60	2.55	2.45	2.64	2.81
33	0.65	2.40	2.38	2.57	2.70
33	0.70	2.30	2.27	2.46	2.58
33	0.80	2.13	2.08	2.26	2.39
33	0.90	1.91	1.89	2.07	2.19
33	1.00	1.73	1.73	1.91	2.03

References

[1] AS/NZS 4673, 2001. Australian/New Zealand Standard, Cold-formed stainless steel structures.

[2] ASDM, 2002. Automotive Steel Design Manual – Revision 6.1 (ASDM), American Iron and Steel Institute, Automotive Applications Committee, Southfield.

[3] ASCE 8-02, 2002. Specification for the design of cold-formed stainless steel Structural members. American Society of Civil Engineers. New York.

[4] Ashraf, M., Gardner, L. & Nethercot, D.A., 2005. Strength enhancement of the corner regions of stainless steel cross-sections. Journal of Constructional Steel Research;61:37-52.

[5] Abaqus, 2009. Hibbit, Karlsson, & Sorensen, Inc. Abaqus/Standard user's manual volumes 1-III and ABAQUS CAE manual. version 6.9-EF1, Pawtucket, USA.

[6] Chan, T.M. & Gardner, L., 2008. Compressive resistance of hot-rolled elliptical hollow sections. Engineering Structures; 30: 522-532.

[7] Chan, T.M., Gardner, L. & Law, K.H., 2010. Structural design of elliptical hollow sections: a review. Proceedings of the Institution of Civil Engineers; 163(SB6) : 391-402.

[8] Ellobody, E. & Young, B., 2005. Structural performance of cold-formed high strength stainless steel columns. Journal of Constructional Steel Research; 61: 1631-1649.

[9] EN 1993-1-4, 2015. Eurocode 3 – Design of steel structures – Part 1-4:. General rules – Supplementary rules for stainless steel. EN 1993-1-4: 2006+A1:2015. CEN.

[10] Gardner, L. & Ministro, A., 2004. Testing and numerical modelling of structural steel oval hollow sections, 04-002-ST. London, Department of civil and environmental engineering, Imperial college.

[11] Gardner, L. & Ashraf, M., 2006. Structural design for non-linear metallic materials. Engineering Structures; 28(6): 926-934.

[12] Haque, T.M., 2011. Elliptical hollow section T and X connections. Master Thesis. Dept of Civil Engineering. University of Toronto, Canada.

[13] Huang, Y. & Young, B., 2012. Material properties of cold-formed lean duplex stainless steel sections. Thin-Walled Structures; 54: 72-81.

[14] Liu, Y. & Young, B., 2003. Buckling of stainless steel square hollow section compression members. Journal of Constructional Steel Research; 59: 165-177.

[15] NAS, 2007. North American Specification for the Design of Cold-Formed Steel Structural Members. Washington, DC: American Iron and Steel Institute.

[16] Parks, M.B. & Yu, W.W., 1987. Structural behavior of members consisting of flat and curved elements. SAE Technical Paper Series 870464.

[17] Parks, M.B. & Yu, W.W., 1989. Local buckling behavior of stiffened curved elements. Thin-Walled Structures; 7:1-22.

[18] Patton, M.L. & Singh, K.D., 2012. Numerical modeling of lean duplex stainless steel hollow columns of square, L-, T-, and +-shaped cross sections under pure axial compression. Thin-Walled Structures; 53: 1–8.

[19] Ramberg, W. & Osgood, W.R., 1943. Description of stress-strain curves by three parameters. Technical Note No. 902, Washington, DC: National advisory committee for aeronautics.

[20] Ruukki.http://www.ruukki.com/Steel/Precision-tubes/Flat-oval-precision-tubes/Form-220-and-370-flat-oval. Retrieved on 15th July 2017.

[21] Saliba, N. & Gardner, L., 2013. Cross-section stability of lean duplex stainless steel welded I-sections. Journal of Constructional Steel Research; 80: 1–14.

[22] Sachidananda, K. & Singh, K.D., 2015. Numerical study of fixed ended lean duplex stainless steel (LDSS) flat oval hollow stub column under pure axial compression. Thin-walled Structures; 96:105-119.

[23] Sachidananda, K. & Singh, K.D., 2017. Structural behaviour of fixed ended stocky lean duplex stainless steel (LDSS) flat oval hollow column under axial compression. Thin-walled Structures; 113: 47-60.

[24] Theofanous, M. & Gardner, L., 2009. Testing and numerical modelling of lean duplex stainless steel hollow section columns. Engineering Structures; 31: 3047-3058.

[25] Theofanous, M., Chan, T.M. & Gardner, L., 2009. Structural response of stainless steel oval hollow section compression members. Engineering Structures; 31: 922-934.

[26] Zhu, J. & Young, B., 2011. Cold-formed-steel oval hollow sections under axial compression. Journal of Structural Engineering; 137:719-727.

[27] Zhu, J. & Young, B., 2012. Design of cold-formed steel oval hollow section columns. Journal of Constructional Steel Research; 71: 26-37.